International Journal of WILDLAND FIRE

Smoke and emissions measurements—RxCADRE 2012

Journal:	*International Journal of Wildland Fire*
Manuscript ID:	WF14166
Manuscript Type:	Research Paper
Date Submitted by the Author:	14-Sep-2014
Complete List of Authors:	Strand, Tara; Scion, Crown Forest Research Institute Gullett, Brian; US Environmental Protection Agency, Office of Research and Development Urbanski, Shawn; USDA Forest Service, RMRS Fire Sciences Laboratory O'Neill, Susan; USDA Forest Service, PNW Research Station Potter, Brian; USDA Forest Service, PNW Research Station Aurell, Johanna; US Environmental Protection Agency, Office of Research and Development; University of Dayton Research Institute, Energy Technology and Materials Division Holder, Amara; US Environmental Protection Agency, Office of Research and Development Larkin, Narasimhan (Sim); USDA Forest Service, PNW Research Station Moore, Mark; USDA Forest Service, PNW Research Station Rorig, Miriam; USDA Forest Service, PNW Research Station
Keyword:	Air, Carbon: emissions, Pollutants: air, Smoke, Smoke: composition

Smoke and emissions measurements—RxCADRE 2012

Tara Strand[A,G], *Brian Gullett*[B], *Shawn Urbanski*[C], *Susan O'Neill*[D], *Brian Potter*[D], *Johanna Aurell*[E,F], *Amara Holder*[B], *Narasimhan Larkin*[D], *Mark Moore*[D], *Miriam Rorig*[D]

[A]Scion, Crown Forest Research Institute, Forestry Building, Forestry Rd, Ilam, Christchurch 8041, New Zealand

[B]US Environmental Protection Agency, Office of Research and Development, Research Triangle Park, NC 27711, USA

[C]USDA Forest Service, Rocky Mountain Research Station, Missoula, MT 59808, USA

[D]USDA Forest Service, Pacific Northwest Research Station, Seattle, WA 98103, USA

[E]National Research Council Postdoctoral Fellow to the U.S. Environmental Protection Agency, Office of Research and Development, National Risk Management Research Laboratory, Research Triangle Park, NC 27711, USA

[F]Currently with: University of Dayton Research Institute, Energy Technology and Materials Division, 300 College Park Dayton, OH 45469, USA

[G]Corresponding author: Email: tara.strand@scionresearch.com

Keywords: smoke, particulate matter, black carbon, emissions factor, combustion efficiency

50 word summary:

Smoke emission measurements were made during grass and forest understory prescribed fires. Instruments deployed on ground, airplane and tethered aerostat platforms measured carbon

species, particulates and optical properties. Smouldering combustion from the forest fire yielded higher carbon monoxide and methane emission factors compared to the grass burn.

Carbon monoxide and methane smouldering emission factors were higher from the forest fire as compared to the grass burn

Abstract

Smoke measurements were made during grass and forest understory prescribed fires as part of a comprehensive program to understand fire and smoke behaviour. Instruments deployed on the ground, airplane and tethered aerostat platforms characterized the smoke plumes through measurements of CO_2, CO, CH_4, and PM, and measurements of optical properties and photographic imaging. The resulting dataset provides a comprehensive, time-resolved characterization of smoke emissions that can be used in modelling programs and to develop methods to mitigate inhalation and visibility hazards. Significant results were found for black carbon emissions, particulate optical properties, and emission factors. Distinctions were observed in aerial and ground-based measurements, with aerial measurements exhibiting smaller particle size distributions and PM emission factors, likely due to particle settling. Black carbon emission factors were similar for both burns and were highest during the initial flaming phase. On average the particles from the forest fire were less light absorbing than those from the grass fires due to the longer duration of smouldering combustion with the forest biomass. CO and CH_4 emission factors were over twice as high for the forest burn compared to the grass burn, corresponding with a lower modified combustion efficiency and greater smouldering combustion.

Introduction

In many regions around the world, fire is an essential ecological process emitting particulate (i.e. Hodzic et al. 2007; Strand et al. 2011) and gaseous compounds (i.e. Goode et al. 1999; Aurell and Gullett 2013) into the atmosphere on a wide variety of spatial and temporal scales, driven by both natural forces and human management decisions. Particulate emissions strongly affect regional visibility (McMeeking et al. 2006), can cause a positive or negative climate forcing (Hobbs et al. 1997), and can cause inhalation health effects (Wegesser et al. 2009). The black carbon fraction of particulates has been found to accelerate Arctic and Greenland ice sheet melting (Bond et al. 2013). The strong spectral variation in light absorption of biomass burning's organic carbon fraction (i.e. brown carbon) contributes to atmospheric warming (Chung et al. 2012) and impacts photochemistry (Li et al. 2011). Gas compounds emitted during biomass burning include greenhouse gases, tropospheric ozone precursors, and other air quality pollutants (Andreae and Merlet 2001). Understanding the impact of these emissions on global climate and regional air quality requires quantifying biomass burning emissions.

Predicting wildland fire emissions requires prediction of fire occurrence and growth, fuel type consumed, and combustion phase such as flaming or smouldering, and each prediction compounds uncertainty (French et al. 2011). Emission factors associated with a fuel type, combustion phase, or both, are used to estimate emissions when combined with mass of fuel consumed. Emission factors have varying ranges of uncertainty depending on the emitted chemical species (Urbanski et al. 2009; Akagi et al. 2011). Several studies have derived emission factors for a variety of North American fuel types, including southeastern USA fuels, using excess concentration data collected from prescribed fires, wildfire measurements, and laboratory studies (i.e. Akagi et al. 2013; Yokelson et al. 2013; Burling et al. 2011). Collectively, these

studies have provided reasonable estimates of emission factors for the primary gas species carbon dioxide, carbon monoxide, methane (CO_2, CO, CH_4, respectively) emitted during biomass burning, and the fuel type with which they are associated. In contrast, for other emitted species, such as particulate matter (PM), uncertainty remains large or unknown (Larkin et al. 2014).

To improve our capability to predict smoke emissions and to model smoke plume concentrations it is necessary to develop a full understanding of the plume's suite of gas and particulate species and their concentrations both near the ground and aloft. Smoke concentration observations combined with measurements of fire behaviour and the fuel type consumed allow for a full time-lapse view of the shift in biomass emissions as it relates to the fire behaviour. The Prescribed Fire Combustion and Atmospheric, Dynamics Research Experiment (RxCADRE) 2012 was designed to collect data needed to advance fire behaviour models and further our understanding of smoke emissions (Ottmar et al., *this issue*). Three prescribed fires were ignited for the purpose of studying smoke emissions and concentrations. These fires consisted of two grass burns and one forest understory fire. Measurements of CO_2, CO, CH_4, fine particulate matter (particles $\leq$ 2.5 micrometres in aerodynamic diameter) ($PM_{2.5}$), particle size distributions, black carbon (BC), and brown carbon (BrC) were collected downwind from the fire, both near the ground and aloft. Emission measurements were compared between ground-based and aerial sampling, as well as among the grass and forest burns. The goal of this paper is to present the smoke emissions and concentration data collected during this study; these data are available for public use from the RxCADRE database (US Department of Agriculture, Forest Service Research 2014).

Methods

Burn and site description

Smoke emissions and plume characteristics were measured during three large burns at Eglin Air Force Base in northwestern Florida, USA. Two large grass fields (L1G and L2G) and the understory of one large forested area (L2F) were lit by drip torch ignition from four-wheel-drive utility task vehicles (UTVs). The goal of the ignition was to develop strips of fire far enough apart that individual head fires ran forward in the classic parabola shape. Detailed site and ignition pattern description is found in Ottmar et al. (*b*) (this issue).

Instruments to photograph the smoke plume and measure emissions were deployed at various ground level locations surrounding the burn units (Fig. 1) and in the air via aircraft and tethered aerostat (Fig. 2). The following sections describe the instruments deployed, sampling methods, and the data obtained during the three burns.

Photography

Still and video cameras were deployed around each of the burns (L1G, L2G, and L2F) to produce a photographic record. Cameras were placed surrounding the burns based on a forecasted wind direction, site accessibility and terrain. Distances from cameras to the burn unit varied in an effort to record as much of the smoke plume and its movement (and various scales of motion) as possible.

Three Canon EOS 5D Mark 3 single lens reflex (SLR) cameras, two Canon EOS 7D SLR cameras, and five Canon Vixia HF R300 video cameras were used (Canon Inc., Japan). These digital cameras were co-located in still/video pairs. Three of the SLR cameras stored all images in raw format, as well as .jpg format, and included devices to determine GPS location of the cameras, and embedded that information in the photograph metadata. The number of images and the size of the files varied based on the duration of the burn. L1G produced 18,000 files (400

GB), L2G produced 23,000 files (820 GB, no video) and L2F produced 13,000 files (200 GB). Figure 3 provides examples of these photographs.

Ground and aerostat instrumentation

Environmental beta attenuation monitors (EBAM, Met One Inc., USA) arrayed around each burn measured 5-min and hourly averages of $PM_{2.5}$ concentrations. To ensure that concentrations were recorded during the burn, even under varying wind conditions, the nine (L1G) and eleven (L2G and L2F) monitors were arrayed in two semi-circles at distances of 20 m and 850 m downwind from the perimeter burns. Background $PM_{2.5}$ concentrations were measured continuously throughout the RxCADRE programme at two locations, one near the burn (850 m from the perimeter) and one further away from the field site (approximately 2.4 km). Air was pulled continuously through an inlet located 2.2 m above ground level (AGL). Leak tests and flow rate tests were conducted before each burn and the flow rate was calibrated if necessary.

A helium-filled tethered aerostat (4.3 m in diameter, Fig. 2) and a ground based UTV each carried a light-weight instrument package termed the "Flyer". The aerostat-Flyer and UTV-Flyer sampling approaches have been described in detail elsewhere (Aurell et al. 2011; Aurell and Gullett 2013). Flyer instruments included SUMMA canisters for CO and CO_2; batch sampling of $PM_{2.5}$ onto a 47-mm diameter Teflon filter (2 µm pore size, constant 10 L min^{-1}); and batch sampling onto quartz filters for elemental carbon and organic carbon (EC and OC) analyses via a modified, thermal-optical analysis (TOA) NIOSH method 5040 (NIOSH 1999) as reported in Khan et al. (2012). Flyers were also equipped with global positioning systems (MTi-G, Xsens, Netherlands) for position and altitude. The aerostat collected emissions at altitudes of 50 to 110 m AGL for the forest burn (L2F) and 45 to 85 m AGL for the grass burn (L2G).

A second, proximally-located, ground-based system made continuous measurements of PM

optical characteristics and BC concentrations during L2G and L2F burns. This system comprised a three-wavelength photoacoustic soot spectrometer (PASS-3, Droplet Measurement Technologies, and USA), a single particle soot photometer (SP2, Droplet Measurement Technologies, and USA), a miniature black carbon monitor AE51 (Magee Scientific), and a DustTrak 8520 (TSI, Inc.). The PASS-3 uses a photoacoustic effect to measure the aerosol absorption coefficient (B_{abs}) and a reciprocal nephelometer to measure the scattering coefficient (B_{scat}) at 405 nm, 532 nm, and 781 nm (Flowers et al. 2010). The SP2 measures size-resolved black carbon concentration by laser-induced incandescence (Schwarz et al. 2006). In addition to these continuous measurements, collocated Teflon and quartz filter samples were taken for determination of $PM_{2.5}$ mass and EC and OC concentrations.

Aircraft instrumentation and sampling

A flight-ready cavity ring-down spectroscopy (CRDS) trace-gas analyser (Picarro, Inc., CA, USA, model G2401-m) was used to take continuous measurements of CO_2, CO, and CH_4 with a data acquisition rate of 2 seconds. Urbanski (2013*a*) provides details on the CRDS instrument and measurement technique. Two point in-flight calibrations using NIST-traceable standards were used to ensure accuracy of the CRDS measurements and quantify the measurement precision. The calibration standards were gas mixtures of CO_2, CO, and CH_4 in Ultrapure air (concentration in ppm ± reported analytical uncertainty: CO_2 = 351 ± 4 and 510 ± 5; CO = 0.092 ± 0.0092 and 3.03 ± 0.06; and CH_4 = 1.493 ± 0.015 and 3.03 ± 0.03) (Scott-Marrin, Inc., USA). The CRDS inflight measurement precision was taken as the 14-s standard deviation while measuring a calibration standard. The three-fire average CRDS measurement precision was 0.251 ppm for CO_2, 0.008 ppm for CO, and 0.005 ppm for CH_4. Calibrations were spaced 25 to 100 minutes apart and were applied to the raw 2-s data points by linearly interpolating the

calibration coefficients. The average drift in the instrument response between calibrations was 0.308 ppm for CO_2, 0.009 ppm for CO, and 0.004 ppm for CH_4.

The measurement platform was a Cessna 337 aircraft. Smoke and ambient air were sampled through a 0.5 in (outside diameter, o.d.) stainless steel inlet located on the pilot window. The CRDS instrument pulled approximately 0.5 standard litres per minute off the sample line. Excess sample flow and the CRDS outflow were exhausted out the rear of the fuselage through a 0.5-in o.d. Teflon line. The aircraft sampling equipment measured fresh smoke emissions, smoke vertical profile, plume height, and smoke dispersion. Measurements of fresh emissions and smoke dispersion were obtained with horizontal flight transects (Fig. 4) in perpendicular and zigzag patterns at distances of up to 25 km downwind from the source. Measurements of the smoke concentration vertical profile (Fig. 5) and the maximum height of the smoke layer were obtained with corkscrew and parking garage flight profiles. Corkscrew profiles, centred on the plume downwind from the burn unit, were taken from above the smoke plume/smoke layer to 150 m above ground level. Parking garage vertical profiles involved short (approximately 10 km) horizontal transects, roughly perpendicular to the long-axis of the smoke plume, taken at multiple altitudes. The parking garage vertical profiles also provide measurements of spatial distribution of smoke emissions and dispersion. Emissions were determined from level-altitude flight segments that began in smoke-free background air, passed through the smoke plume, and then re-entered the background air. A section of each flight segment prior to plume entry provided the background measurements that were used to calculate the excess mixing ratios. The background CO provided a baseline to identify the smoke plume entry and exit points and selection of the smoke sample data points.

Data analyses

Hourly and 5-min surface $PM_{2.5}$ concentration data were similar for L1G and L2G, and L1G data were plotted. For L2F, hourly $PM_{2.5}$ concentrations measured from all monitors were placed into a boxplot, which represented the spread of values measured during each hour of the burn.

Emission factors (EF) for pollutant X, EF_X (in units of mass of X per mass of dry fuel consumed), were calculated for each smoke sample using the carbon mass balance method (Eqn. 1) as found in Yokelson et al. (1999) and Laursen et al. (1992). The carbon (C) volatized during combustion was calculated from mixing ratios of simultaneously-sampled, background-corrected C containing species, ΔX ($\Delta X = X_{smoke} - X_{background}$), and the C fraction ($F_c$) in the fuel biomass. A value of 0.5 was used for F_c based on analysis of the forest litter (Table 1) and was estimated to be the same for the grass units. Previous biomass burning emission studies have found F_c to range between 0.45 and 0.55 for the vegetation types burned in this study (Burling et al. 2010).

$$EF_X = F_c \times 1000\ (g\,kg^{-1}) \times \frac{MM_X}{12} \times \frac{\Delta X}{\Delta C_{CO_2} + \Delta C_{CO} + \Delta C_{CH_4}} \quad (1)$$

where ΔC_i are the excess mass mixing ratios of C in each emitted species X; MM_X is the molar mass of X (g mole^{-1}), and 12 is the molar mass of carbon (g mole^{-1}).

For the airplane measurements, CO_2, CO, and CH_4 were used in the C balance calculation as described in Urbanski 2013*a*. The neglect of other carbon-containing species has less than a 5% effect on the EF (Urbanski 2013*b*). The ground- and aerostat-based measurements presented in this paper did not include CO and CH_4 and therefore only CO_2 was used to calculate EFs from these data. The CRDS data show that CO and CH_4 comprised ~5% and ~10% of the measured C (sum of CO_2, CO, and CH_4) for the grass burns and forest fire, respectively. These results and

consideration of previous studies (Urbanski 2013*b*; Yokelson et al. 2013) indicate that using only CO_2 in the C balance calculations would inflate EF by less than 15%, a value within the total error of the method and likely the reproducibility of the event.

Modified combustion efficiency (MCE), a measure of the fire behaviour's phase, was calculated as:

$$\frac{\Delta CO_2}{\Delta CO+\Delta CO_2}, \quad (2)$$

using the CO and CO_2 concentrations collected by the SUMMA canisters and continuous measurements in the airplane.

For the DustTraks, custom correction factors were calculated according to the manufacturer's recommendations (TSI 2010) for DustTraks 8520 and DRX by dividing the average continuous $PM_{2.5}$ concentration by the $PM_{2.5}$ batch filter concentration collected during the same time period. The correction factors for DustTrak DRX for grass and forest field burns were 1.6 and 2.4, respectively. The DustTrak 8520 had correction factors of 1.9 and 0.91 for forest and grass burns, respectively. The BC and BrC data from the AE51 and AE52 were post-processed for noise using the optimized noise-reduction averaging algorithm program (Hagler et al 2011).

The single scattering albedo (SSA) was calculated for each of the three wavelengths (λ) measured by the PASS-3:

$$SSA = \frac{\beta_{scat}}{\beta_{scat}+\beta_{abs}}, \quad (2)$$

where β_{scat} is the scattering coefficient and β_{abs} is the absorption coefficient. Low values of SSA indicate that the BC fraction dominates the PM resulting in positive climate forcing. The absorption angstrom exponent (AAE) describes the spectral variation of the absorption:

$$AAE_{1-2} = -\frac{\ln(\beta_{abs}(\lambda_1))/\ln(\beta_{abs}(\lambda_2))}{\ln(\lambda_1)/\ln(\lambda_2)}, \quad (3)$$

where $\beta_{abs}(\lambda_1)$ is the absorption coefficient at wavelength 1 (λ_1), and $\beta_{abs}(\lambda_2)$ is the absorption coefficient at wavelength 2 (λ_2). An AAE value near 1 is indicative of urban pollution (i.e. diesel soot), while values larger than one are associated with brown carbon from biomass burning (Clarke et al. 2007). The mass-specific absorption coefficient (MAC), B_{abs}(781nm)/EC, was calculated for black carbon.

Results

Photography

The still and video photographs have not been analysed in any detail, but casual observation reveals some valuable information on the potential and challenges of analysing them. The ability to position multiple cameras around a prescribed burn is constrained by distance from the fire, clear viewpoints, relationship to other cameras, and sun angle relative to direction of the camera at the time of the burn. Obtaining good perspectives of the smoke plume from every camera becomes difficult. For example, the plume is both visible (Fig. 3*a*) and washed out (Fig. 3*b*) as viewed by two different cameras at the same time. Further detailed analysis of the photographs will require determining what can be measured from individual camera records, or from the video images, as it appears comparison of images from multiple cameras is not feasible.

259

260 *Ground and aerostat measurements*

261 Fire ignition duration, fuel type, and $PM_{2.5}$ concentration averaging period dictated the duration
262 and magnitude of smoke impacts downwind from the EBAMs. The grass burns resulted in higher
263 five-minute concentrations while the forest understory burn resulted in higher hourly averages of
264 $PM_{2.5}$ concentrations, which lasted for several hours due to evening smouldering. For the grass
265 burns, which were short in duration, the $PM_{2.5}$ monitors measured elevated concentrations for
266 only one to two hours (Fig. 6). During L1G burn, three of the nine deployed EBAMs were
267 impacted by the smoke plume with 5-min and hourly maximum $PM_{2.5}$ concentration values of
268 approximately 2300 μg m^{-3} and 500 μg m^{-3}, respectively. Both maximums occurred 50 m from
269 the burn perimeter. During the L2F burn, $PM_{2.5}$ concentrations were measured for approximately
270 10 hours at all eleven EBAMs. The box plots of hourly $PM_{2.5}$ concentrations demonstrate the
271 range of $PM_{2.5}$ concentration values measured during the onset and passage of the primary smoke
272 plume and also during the smouldering phase, which extended into the evening (Fig. 7). The
273 maximum hourly $PM_{2.5}$ concentration value was approximately 1100 μg m^{-3} and the maximum
274 5-min $PM_{2.5}$ concentration was approximately 1500 μg m^{-3} (not shown).

275 Emission factors for $PM_{2.5}$ ($EFPM_{2.5}$) from ground and aerostat measurements for L2F (Fig.
276 8) (Table 2) were higher (20 and 23 g kg^{-1}) than those derived in a previous study from the same
277 location and sampling team (14 g kg^{-1}) (Aurell and Gullett 2013), possibly due to differences in
278 biomass characteristics. During this current study, a slightly higher emission factor was shown
279 for L2F compared to L2G. Aerostat and ground $PM_{2.5}$ concentrations were similar, with the
280 ground measurements about 10% higher. Particle size results showed that ≥98% of the
281 particulate matter from both burns was comprised of PM_1 (particles ≤ 1 micrometre in

aerodynamic diameter) (Fig. 8). The particle distribution for L2F showed a higher percentage of PM_1 compared to L2G. Data were collected from a higher altitude during L2F (50 to 110 m AGL) compared to L2G (2 m AGL), suggesting that both biomass type and particle settling effects may have been responsible for these size differences, the latter theory supporting the slightly higher EFs measured on the ground versus those from the air (Fig. 8).

BC (light-absorbing aerosol in the infrared spectrum) and BrC (light-absorbing organic matter aerosols found in the ultraviolet spectrum) emission factors (EFBC, EFBrC) were 0.89 to 1.4 g kg^{-1} and 0.92 to 1.8 g kg^{-1}, respectively (Fig. 9). The EFBC are similar to those previously reported from forest understory burns in the same area and sampling team using the same methods (1.4 and 2.7 g kg^{-1}) (Aurell and Gullett, 2013). No differences in EFBC between forest and grass burns were detected.

Modified combustion efficiency (MCE) values were compared to simultaneously-sampled EFBC (Fig. 10). The ground-sampled EFBC derived from L2F agreed with previously reported data from forest understory burns (Aurell and Gullett, 2013), showing higher EFBC with increased MCE. The aerostat-lofted EFBC (2.4 g kg^{-1}) was higher than that from the ground (1.4 g kg^{-1}) for the same MCE, perhaps indicating a bias of BC toward smaller particles, which were found to be in greater quantity aloft. Derived EFBC from L2G were lower than those derived from L2F for the same range of MCE.

There were subtle differences in the characteristics of particles emitted from L2G, compared with L2F. L2G emissions exhibited a higher EC/$PM_{2.5}$ ratio and lower SSA values compared to L2F (Table 2). Emissions from L2F had a slightly larger AAE, indicating a larger brown carbon contribution compared to L2G. The L2F mass-specific absorption coefficient was also elevated which suggests an internally mixed aerosol where the organic carbon has condensed onto the

surface of elemental carbon particles and amplified their absorption (Lack and Cappa 2010). The black carbon size distribution also differed between the L2F and L2G (Fig. 11). The BC mass median diameter (MMD) from L2F was 20% larger than that measured during L2G. Overall, the particle characteristics suggest that L2F had a larger smouldering contribution compared to L2G.

The BC fraction and the PM optical properties varied over the duration of the L2F fire (Fig. 12). Early in the fire there was a large spike in the $BC/PM_{2.5}$ ratio, which corresponded with the lowest observed SSA of 0.58. As the burn progressed the $BC/PM_{2.5}$ ratio slowly decreased as SSA slowly increased. This trend corresponds with the decrease in MCE that was measured with the aircraft and demonstrates the relationship between BC emissions and the phase of the fire, with more BC emitted during the flaming phase.

Aircraft measurements

All three fires (L1G, L2G, and L2F) were sampled from ignition until smoke produced by the smouldering fire was no longer lofted high enough to be sampled by the aircraft (approximately 160 m AGL). The sampling time period covered 90 minutes (L1G) to 150 minutes (L2F) during which 10 to 30 smoke samples were collected for each fire. The smoke emission samples were obtained between 700 m and 14000 m downwind from the burn units at altitudes between 160 m and 1530 m above mean sea level (AMSL). Mixing ratios found in a smoke sample from the L2F fire are shown in Fig. 13. Supplemental Table S1 gives the emission factors, MCE, ΔX, altitude, and estimated time of emission (ETE) for each smoke sample. The horizontal distance covered by each sample and the number of 2-s data points varied with the flight profile, aircraft speed, source strength, and dispersion conditions. The typical aircraft groundspeed during smoke sampling was 64 m s^{-1}. The ETE were derived from the wind speed at the altitude of the sample

and the average distance of the sample leg from the centroid of the burn unit. The wind speed data from the post-fire atmospheric soundings (Clements et al. *this issue*) were used in the ETE calculations.

The fire average MCE and emission factors for the grass-dominated units (L1G and L2G) were in close agreement with differences of <1% for MCE and $EFCO_2$, and approximately 3% and 11% for EFCO and $EFCH_4$, respectively (Table 3). While the averages were similar, the variance of MCE and the emissions factors for L1G were twice that of L2G, indicating a wider range of fire behaviour in which the samples were taken. The forested unit burned with a significantly lower MCE and had EFCO and $EFCH_4$ that were 2 and 2.6 times the grass unit averages, respectively (Table 3).

During the L2F fire $EFCH_4$, and to lesser extent MCE, varied with ETE (Fig. 14) with $EFCH_4$ increasing over the course of the fire while MCE decreased. This behaviour is consistent with a greater contribution from smouldering combustion during the later stages of the fire. However, the different temporal patterns in MCE and $EFCH_4$ (not shown) suggest they relate differently to fuel components and the combustion process. There was no correlation of $EFCH_4$ (or MCE) with altitude or distance from the source indicating that the trend was not an artefact of the smoke sampling pattern nor length of time the smoke was in the atmosphere before sampling. For the L2F fire a linear least square regression of $EFCH_4$ vs. MCE yielded the fit: $y = 54.4 – 55.3x$ ($R^2 = 0.42$). There was not a significant correlation between $EFCH_4$ and MCE for either the L1G or the L2G fire.

Discussion and Conclusion

$PM_{2.5}$ ground concentrations

Concentrations of $PM_{2.5}$ during both grass burns differed little both with elevated concentrations

over a short duration but with peaks greater than the forest understory burn. The understory forest burn produced elevated concentrations that lasted well after the cessation of ignition as the fuels smouldered. Maximum hourly $PM_{2.5}$ concentrations were higher than that found during the grass burns, however maximum five-minute $PM_{2.5}$ concentrations were lower than the grass burns. This combination demonstrates slower pace of the L2F burn compared to the L1G and L2G burns, as well as the quantity of L2F smouldering fuels. Differences between the aerostat and ground $PM_{2.5}$ concentrations measured during L2G and L2F were small with slightly higher concentrations measured near the ground. Data from these burns suggest that larger particles may settle out with altitude placing larger particles closer to the ground.

Emission factors

The fuels consumed in the L1G and L2G fires largely consisted of grass and forbs (78% and 76%, respectively) with litter and shrubs constituting the balance (Ottmar et al. *this issue*). In contrast, grass and forb consumption was negligible in L2F, where litter (pine and hardwood), dead woody debris, and shrubs accounted for 79%, 15%, and 6% of the total fuel consumed, respectively (Ottmar et al. *this issue*). The fuel consumption measurements suggest that while grass and litter are both classified as fine fuels (fuel particles with a high surface to volume ratio), the latter burned with a significantly lower MCE (and produced higher EFCO and $EFCH_4$). Urbanski (2013b) examined MCE and fuel consumption data from 18 prescribed fires and found that when fuel consumption was dominated by fine fuels (litter, grasses, shrubs, and fine woody debris) high MCE was favoured. The fires in this study were dominated by fine fuel consumption but burned with significantly different MCE and produced different emission factors suggests that the composition and characteristics of fine fuels (grass and forbs vs. litter

and woody debris) may be an important factor influencing emissions.

The grass-dominated units burned with high MCE and low EFCO and $EFCH_4$ in contrast to the forested unit, a finding that is consistent with previous studies. Comparing the L2F results with previous field studies of emissions from prescribed fires in pine-dominated forests of the Southeastern U.S.A (Fig. 15) the L2F MCE is on the low end of the fire average values reported by Akagi et al. (2013), Burling et al. (2011), and Urbanski et al. (2009). Six fires included as grasslands and shrublands in Urbanski et al. (2009) were actually forest understory burns (EB1, EB2, FL5, SC9, FS1, and ICI3). We have included these six fires in our analysis. In terms of carbon, CH_4 is the dominant organic gas released by prescribed fires and so we compare our $EFCH_4$ with that reported in these three previous field studies. Of these the $EFCH_4$ of only one fire exceeds our L2F $EFCH_4$ and that fire's MCE is substantially lower than the average of the 34 fires reported in these three studies (0.906 vs. 0.934). Interestingly, our $EFCH_4$ value (4.32 g kg^{-1}) is close to the value predicted by the $EFCH_4$ vs. MCE regression equation (4.44 g kg^{-1}) reported in Akagi et al. (2013). Conversely, using all thirty-four previously published fires the $EFCH_4$ vs. MCE linear equation ($y = 47.3 – 48.3x$; $R^2=0.47$) predicts an $EFCH_4$ of 3.54 g kg^{-1} for L2F (with an MCE of 0.906), approximately 20% below the observed value.

We may compare our results from the grass burns (L1G and L2G) with eight grassland burns (EP1, EP2A, EP2B, MI1, MN1, MN2, MN3, and MN4) reported in Urbanski et al. (2009). L1G and L2G fires have similar MCE and emission factor values to these eight grassland fires, which have an average MCE of 0.945 and corresponding $EFCH_4$ of 1.95 g kg^{-1}. Our values are 10% (L1G) and 19% (L2G) below this grassland fire average. These small differences are attributed to the MCE. A linear least square regression, using the eight grassland fires, of $EFCH_4$ vs. MCE yields the fit: $y = 54.0 – 55.0x$ ($R^2 = 0.92$). This equation predicts $EFCH_4$ of 1.75 g kg^{-1} for L1G

398 and 1.59 g kg^{-1} for L2G. This agrees with those measured in our study.

399

400 *Particulate characteristics*

401 There are a limited number of in situ measurements of fresh biomass plume optical properties
402 and to our knowledge none for the southeastern USA. Our single scattering albedos for L2G and
403 L2F fall among the range of 0.8 to 0.9 (at 540 nm) reported for wildfires and prescribed burns in
404 the Western USA and Canada (Radke et al. 1988, 1991). A lower SSA for the grass-dominated
405 unit compared to the forested unit was also observed by Reid and Hobbs (1998), who measured
406 an SSA of 0.76 for grass and an SSA of 0.84 for smouldering slash and standing forest fires in
407 Brazil. SSA values from different fuels in the laboratory measurements have been mixed, with
408 no consistent difference between grasses and trees (litter and woody debris) or shrubs (Lewis et
409 al 2008, Mack et al. 2010).

410 The AAE measured during the L2G and L2F burns were somewhat higher than other
411 measurements in fresh plumes and indicate that there may have been more BrC or BrC with
412 varying optical properties. For example, Corr et al. (2012) measured 1.38 (470 to 573 nm) in a
413 fresh boreal plume compared to the 2.44 to 3.01 (405 to 532 nm) we observed for the L2G and
414 L2F burns, respectively. Laboratory measurements by Lewis et al. (2008) found a large range of
415 AAE of 0.86 to 3.48 (405 to 870 nm), which depended on the fuel. However, it is difficult to
416 compare AAE across studies as different measurement methods can provide very different
417 results (Corr et al. 2012) and these results are dependent upon the wavelength range investigated
418 as biomass burning PM exhibit increasing AAE with decreasing wavelength (Lewis et al. 2008;
419 Sandradewi et al. 2008; Corr et al. 2012).

420 The black carbon MMD of 209 nm measured for the forested unit is similar to the average
421 193 nm found in fresh prescribed and wildfire plumes in California (Sahu et al. 2012), 187 nm

for fresh boreal wildfire plumes (Kondo et al. 2011), and 210 nm for plumes (likely brush fires) over Texas (Schwarz et al. 2008). We have assumed a black carbon density of 1.8 g cm^{-3} for our calculations, which makes our MMD approximately 3% larger than that previously measured, where the assumed density was 2 g cm^{-3}. The difference in sizes between the fires at L2G and L2F (Fig. 10) are approximately within the variation observed by Kondo et al. (2011) in fresh and aged boreal plumes. Although Kondo et al. (2011) observed a slight trend of decreasing black carbon size with increasing MCE, they could not account for the impact of different vegetation.

RxCADRE data

A wide array of smoke measurements were made on the large grass and forest burns during the RxCADRE 2012 field campaign. The RxCADRE dataset was collected for use by all who require such a dataset to test theory, develop fire behaviour models, and to evaluate smoke prediction models. The combination of ground-based measurements at various distances from the fires, airborne measurements at multiple heights and distances, and measuring a variety of smoke components makes for a robust dataset and provides guidance for future measurement efforts. Pairing the collected smoke emissions and concentration data with the fuel, consumption, fire behaviour and meteorological measurements collected during the burns allows for an understanding of the shift in biomass emissions as they relate to the fire behaviour. These factors need to be accounted for when developing smoke models for use in defining visibility, inhalation health effects, and climate issues.

Acknowledgements

This work was funded by the Joint Fire Science Program (Project #11-2-1-11), the Strategic Environmental Research and Development Program (Dr. John Hall) and the U.S. EPA Office of Research and Development. This research was performed while Johanna Aurell held a National Research Council Research Associateship Award at the U.S. EPA/NRMRL. We would like to thank Dave Hubble our mission Cessna 337 pilot and Aaron Knobloch of USFS Southern Region for his support in facilitating the airplane arrangements. Contributing EPA personnel included Chris Pressley, Bill Squier, Bill Mitchell, Michael Hays, and Robert Black (Oak Ridge Institute for Science and Education [ORISE] post-doctoral fellow). Aerostat operations were handled by Rob Gribble (ISSI, Inc.). Jeff Blair of AethLabs donated use of the AE-52. We also thank Candace Krull for her assistance with preparing field equipment prior to the study and Gary Curcio for contributing instrumentation, expertise and aid in deploying the equipment. We also give a special thanks to Scott Pokswinski (aka Daisycutter) who watched out for us while at the field site.

The use of trade or firm names in this publication is for reader information and does not imply endorsement by the U.S. Department of Agriculture and Environmental Protection Agency of any product or service.

References

Akagi SK, Yokelson RJ, Wiedinmyer C, Alvarado MJ, Reid JS, Karl T, Crounse JD, Wennburg PO (2011) Emission factors for open and domestic biomass burning for use in atmospheric models. *Atmospheric Chemistry and Physics Discussion* **10**, 27523–27602. doi: 10.5194/acp-11-4039-2011

Akagi SK, Yokelson RJ, Burling IR, Meinardi S, Simpson I, Blake DR, McMeeking GR, Sullivan A, Lee T, Kreidenweis S, Urbanski S, Reardon J, Griffith DWT, Johnson TJ, Weise

DR (2013) Measurements of reactive trace gases and variable O_3 formation rates in some South Carolina biomass burning plumes. *Atmospheric Chemistry and Physics* **13**, 1141–1165. doi:10.5194/acp-13-1141-2013

Aurell J, Gullet BK (2013) Emission factors from aerial and ground measurements of field and laboratory forest burns in the southeastern US: $PM_{2.5}$, black and brown carbon, VOC, and PCDD/PCDF. *Environmental Science & Technology* **47**, 8443–8452. doi: 10.1021/es402101k

Aurell J, Gullet BK, Pressley, Tabor D, Gribble R (2011) Aerostat-lofted instrument and sampling method for determination of emissions from open area sources. *Chemosphere* **85,** 806–811. doi: 10.1016/j.chemosphere.2011.06.075

Andreae MO, Merlet P (2001) Emission of trace gases and aerosols from biomass burning. *Global Biogeochemical Cycles* **15**, 955–966. doi: 10.1029/2000GB001382

Bond TC, Doherty SJ, Fahey DW, Forster PM, Bernsten T, DeAngelo BJ, Flanner MG, Ghan S, Kärcher B, Koch D, Kinne S, Kondo Y, Quinn PK, Sarofim MC, Schulz M, Venkataraman C, Zhang H, Zhang S, Bellouin N, Guttikunda SK, Hopke PK, Jacobson MZ, Kaiser JW, Klimont Z, Lohmann U, Schwarz JP, Shindell D, Storelvmo T, Warren SG, Zender CS (2013) Bounding the role of black carbon in the climate system: a scientific assessment. *Journal of Geophysical Research: Atmospheres* **118**, 5380–5552. doi: 10.1002/jgrd.50171

Burling IR, Yokelson RJ, Griffith DWT, Johnson TJ, Veres P, Roberts JM, Warneke C, Urbanski SP, Reardon J, Weise DR, Hao WM, de Gouw J (2010) Laboratory measurements of trace gas emissions from biomass burning of fuel types from the southeastern and southwestern United States. *Atmospheric Chemistry and Physics* **10**, 1115–11130. doi: 10.5194/acp-10-11115-2010

Burling IR, Yokelson RJ, Akagi SK, Urbanski SP, Wold CE, Griffith DWT, Johnson TJ, Reardon J, Weise DR (2011) Airborne and ground-based measurements of the trace gases and particles emitted by prescribed fires in the United States. *Atmospheric Chemistry and Physics* **11**, 12197–12216. doi 10.5194/acp-11-12197-2011

Chung CE, Ramanathan V, Decremer D (2012) Observationally constrained estimates of carbonaceous aerosol radiative forcing. *Proceedings of the National Academy of Sciences* **109**, 11624–11629. doi: 10.1073/pnas.1203707109

Clarke A, McNaughton C, Kapustin V, Shinozuka Y, Howell S, Dibb J, Zhou J, Anderson B, Brekhovskikh V, Turner H, Pinkerton M (2007) Biomass burning and pollution aerosol over North America: organic components and their influence on spectral optical properties and humidification response. *Journal of Geophysical Research: Atmospheres* **112**, D12S18. doi: 10.1029/2006JD007777

Corr CA, Hall SR, Ullmann K, Anderson BE, Beyersdorf AJ, Thornhill KL, Cubison MJ, Jimenez JL, Wisthaler A, Dibb JE (2012) Spectral absorption of biomass burning aerosol determined from retrieved single scattering albedo during ARCTAS. *Atmospheric Chemistry and Physics* **12**, 10505–10518. doi: 10.5195/acp-12-10505-2012

Flowers BA, Dubey MK, Mazzoleni C, Stone EA, Schauer JJ, Kim SW, Yoon SC (2010) Optical-chemical-microphysical relationships and closure studies for mixed carbonaceous aerosols observed at Jeju Island; 3-laser photoacoustic spectrometer, particle sizing, and filter analysis. *Atmospheric Chemistry and Physics* **10**, 10387–10398. doi: 10.5194/acp-10-10387-2010

French NH, de Groot WJ, Jenkins LK, Rogers BM, Alvarado E, Amiro B, de Jong B, Goetz S, Hoy E, Hyer E, Keane R, Law BE, McKenzie D, McNulty SG, Ottmar R, Pérez-Salicrup

DR, Randerson J, Robertson KM, Turetsky M (2011) Model comparisons for estimating carbon emissions from North American wildland fire. *Journal of Geophysical Research: Biogeosciences* **116**, G00K05. doi: 10.1029/2010JG001469

Goode J G, Yokelson RJ, Susott R A, Ward DE (1999) Trace gas emissions from laboratory biomass fires measured by open-path Fourier transform infrared spectroscopy: fires in grass and surface fuels. *Journal of Geophysical Research: Atmospheres* **104**, 21237–21245. doi: 10/10291999JUD900360

Hagler GSW, Yelverton TLB, Vedantham R, Hansen ADA, Turner JR (2011) Post-processing method to reduce noise while preserving high time resolution in aethalometer real-time black carbon data. *Aerosol and Air Quality Research* **11**, 539–546. doi: 10.4209/aaqr.2011.0055

Hobbs PV, Reid JS, Kotchenruther RA, Ferek RJ, Weiss R (1997) Direct radiative forcing by smoke from biomass burning. *Science* **275**, 1777–1778. doi: 10.1126/science.275.5307.1777

Hodzic A, Madronich S, Bohn B, Massie S, Menut L, Wiedinmyer C (2007) Wildfire particulate matter in Europe during summer 2003: mesoscale modeling of smoke emissions, transport and radiative effects. *Atmospheric Chemistry and Physics* **7**, 4043–4064. doi: 10.5194/acp-7-4043-2007

Khan B, Hays MD, Geron C, Jetter J (2012) Differences in the OC/EC ratios that characterize ambient and source aerosols due to thermal-optical analysis. *Aerosol Science and Technology* **46**, 127–137. doi: 10.1080/02786826.2011.609194

Kondo Y, Matsui H, Moteki N, Sahu L, Takegawa N, Kajino M, Zhao Y, Cubison MJ, Jimenez JL, Vay S, Diskin GS, Anderson B, Wisthaler A, Mikoviny T, Fuelberg HE, Blake DR, Huey G, Weinheimer AJ, Knapp DJ, Brune WH (2011) Emissions of black carbon, organic, and inorganic aerosols from biomass burning in North America and Asia in 2008. *Journal of*

Geophysical Research: Atmospheres **116**, D08204. doi: 10.1028/2010JD015152

Lack DA, Cappa CD (2010) Impact of brown and clear carbon on light absorption enhancement, single scatter albedo and absorption wavelength dependence of black carbon. *Atmospheric Chemistry and Physics* **10**, 4207–4220. doi: 10.5194/acp-10-4207-2010

Larkin NK, Raffuse SM, Strand TM (2014) Wildland fire emissions, carbon, and climate: US emissions inventories. *Forest Ecology and Management* **317**, 61–69. doi: 20/1016/j.foreco.2013.09.012

Laursen KK, Ferek R, Hobbs P, Rasmussen RA (1992) Emission factors for particles, elemental carbon, and trace gases from the Kuwait oil fires. *Journal of Geophysical Research: Atmospheres* **97**, 14491–14497. doi: 10.1029/92JD01370

Lewis K, Arnott WP, Moosmüller H, Wold CE (2008) Strong spectral variation of biomass smoke light absorption and single scattering albedo observed with a novel dual-wavelength photoacoustic instrument. *Journal of Geophysical Research: Atmospheres* **113**, D16203. doi: 10.1029/2007JD009699

Li G, Bei N, Tie X, Molina LT (2011) Aerosol effects on the photochemistry in Mexico City during MCMA-2006/MILAGRO campaign. *Atmospheric Chemistry and Physics* **11**, 5169–5182. doi: 10.5194/acp-11-5169-2011

Mack LA, Levin EJT, Kreidenweis SM, Obrist D, Moosmüller H, Lewis KA, Arnott WP, McMeeking GR, Sullivan AP, Wold CE, Hao W-M, Collett JL, Malm WC (2010) Optical closure experiments for biomass smoke aerosols. *Atmospheric Chemistry and Physics* **10**, 9017–9026. doi: 10.5194/acp-10-9017-2010

McMeeking GR, Kreidenweis SM, Lunden M, Carrillo J, Carrico CM, Lee T, Herckes P, Engling G, Day DE, Hand J, Brown N, Malm WC, Collett Jr JL (2006) Smoke-impacted

regional haze in California during the summer of 2002. *Agricultural and Forest Meteorology* **137**, 25–42. doi: 10.1016/j.agrformet.2006.01.011

NIOSH (1999) Method 5040: Elemental carbon (diesel particulate), Issue 3 (interim), NIOSH Manual of Analytical Methods, 4th ed., 30 September, 1999.

Radke LF, Hegg DA, Lyons JH, Brock CA, Hobbs PV, Weiss RE, Rassmussen R (1988) Airborne measurements on smokes from biomass burning. In 'Aerosols and climate'. (Eds. PV Hobbs, MP McCormick), pp. 411–422. (Deepak Publishing: Hampton, VA)

Radke LF, Hegg DA, Hobbs PV, Nance JD, Lyons JH, Larsen KK, Weiss RE, Regan PJ, Ward DE (1991) Particulate and trace emissions from large biomass fires in North America. In 'Global biomass burning: Atmospheric, climate, and biospheric implications.' (Ed JS Levine) pp. 209–224. (MIT Press: Cambridge, MA)

Reid JS, Hobbs PV (1998) Physical and optical properties of young smoke from individual biomass fires in Brazil. *Journal of Geophysical Research: Atmospheres* **103**, 32013–32030. doi:10.1029/98JD00159

Sahu LK, Kondo Y, Moteki N, Takegawa N, Zhao Y, Cubison MJ, Jimenez JL, Vay S, Diskin GS, Wisthaler A, Mikoviny T, Huey LG, Weinheimer AJ, Knapp DJ (2012) Emission characteristics of black carbon in anthropogenic and biomass burning plumes over California during ARCTAS-CARB 2008. *Journal of Geophysical Research: Atmospheres* **117**, D16302. doi: 10.1029/2011JD017401

Sandradewi J, Prevot ASH, Weingartner E, Schmidhauser R, Gysel M, Baltensperger U (2008) A study of wood burning and traffic aerosols in an alpine valley using a multi-wavelength aethalometer. *Atmospheric Environment* **42**, 101–112. doi: 10.1016/j.atmosenv.2007.09.034

Schwarz JP, Gao RS, Fahey DW, Thomson DS, Watts LA, Wilson JC, Reeves JM, Darbeheshti

M, Baumgardner DG, Kok GL, Chung SH, Schulz M, Hendricks J, Lauer A, Karcher B, Slowik JG, Rosenlof KH, Thompson TL, Langford AO, Loewenstein M, Aikin KC (2006) Single-particle measurements of midlatitude black carbon and light-scattering aerosols from the boundary layer to the lower stratosphere. *Journal of Geophysical Research: Atmospheres* **111**, D16207

Schwarz JP, Gao RS, Spackman JR, Watts LA, Thomson DS, Fahey DW, Ryerson TB, Peischl J, Holloway JS, Trainer M, Frost GJ, Baynard T, Lack DA, de Gouw JA, Warneke C, Del Negro LA (2008) Measurement of the mixing state, mass, and optical size of individual black carbon particles in urban and biomass burning emissions. *Geophysical Research Letters* **35**, L13810.

Strand T, Larkin N, Rorig M, Krull C, Moore M (2011) $PM_{2.5}$ measurements in wildfire smoke plumes from fire seasons 2005–2008 in the northwestern United States. *Journal of Aerosol Science* **42**, 143–155.

TSI (2010) Model 8520 DustTrack aerosol monitor operation and service manual, 1980198 rev. 8, June 2010. http://www.tsi.com/uploadedfiles/_site_root/products/literature/manuals/1980198S-8520.pdf (14 March 2014)

Urbanski SP, Baker SP, Hao WM (2009) Chemical composition of wildland fire emissions. In: 'Wildland fires and air pollution'. (Eds. A Bytnerowicz, M Arbaugh, A Riebau, and C Anderson), pp. 79–107. (Elsevier: United Kingdom)

Urbanski SP (2013*a*) Combustion efficiency and emission factors for wildfire-season fires in mixed conifer forests of the northern Rocky Mountains. US. *Atmospheric Chemistry and Physics* **13**, 7241–7262.

607 Urbanski SP (2013*b*) Wildland fire emissions, carbon, and climate: emission factors. *Forest*
608 *Ecology and Management*. In Press.
609 US Department of Agriculture, Forest Service Research (2014) Research data archive.
610 http://www.fs.usda.gov/rds/archive/Product/RDS-2014-xxxx. [04 August 2014]
611 Wegesser TC, Pinkerton KE, Last JA (2009) California wildfires of 2008: coarse and fine
612 particulate matter toxicity. *Environmental Health Perspectives* **117**, 893–897.
613 Yokelson R, Goode J, Ward D, Susott R, Babbit R, Wade D, Bertschi I, Griffith D, Hao W
614 (1999) Emissions of formaldehyde, acetic acid, methanol, and other trace gases from biomass
615 fires in North Carolina measured by airborne Fourier transform infrared spectroscopy.
616 *Journal of Geophysical Research: Atmospheres* **104**, 30109–30125.
617 Yokelson RJ, Burling IR, Gilman JB, Warneke C, Stockwell CE, de Gouw J, Akagi SK,
618 Urbanski SP, Veres P, Roberts JM, Kuster WC, Reardon J, Griffith DWT, Johnson TJ,
619 Hosseini S, Miller JW, Cocker III DR, Jung H, Weise DR (2013) Coupling field and
620 laboratory measurements to estimate the emission factors of identified and unidentified trace
621 gases for prescribed fires. *Atmospheric Chemistry and Physics* **13**, 89–116.
622

623 **Tables**

624

625 **Table 1. Ultimate analyses of the forest litter collected before the forest understory surface**

626 **fire (L2F)**

	Forest litter
Loss of mass due to water evaporation when drying (%)	17.4
Carbon (F_c) (%)	49.6
Chlorine (ppm)	849
Oxygen (%)	42.4
Hydrogen (%)	6.3
Nitrogen (%)	<0.5
Sulphur (%)	0.0585

627

628

Table 2. $PM_{2.5}$, BC, BrC, EC, and OC emission factors and PM single scattering albedo (SSA), absorption angstrom exponent (AAE), and BC mass-specific absorption coefficient (MAC)

Compound	Units	Grass burn (L2G)		Forest burn (L2F)	
		Ground	Aerostat	Ground	Aerostat
Filter $PM_{2.5}$	g kg^{-1}	18	14	23±1.8[c]	20
Continuous $PM_{2.5}$	g kg^{-1}	20	15	25	24
Continuous BC[a]	g kg^{-1}	1.1	0.91	0.89	1.4
Continuous BrC	g kg^{-1}	1.8	NS	NS	0.92
Filter EC	g kg^{-1}	0.62	0.56	0.39±0.16[c]	0.46
Filter OC	g kg^{-1}	7.0	6.5	15±1.8[c]	11.3
$BC/PM_{2.5}$[b]	mass ratio (%)	6.8	7.0	3.6±0.67[c]	7.0
$EC/PM_{2.5}$	mass ratio (%)	3.5	3.9	1.6±0.54[c]	2.3
SSA 405 nm		0.78		0.83	
SSA 532 nm		0.83		0.87	
SSA 781 nm		0.76		0.87	
AAE (405–532 nm)		2.60		2.81	
AAE (532–781 nm)		2.09		1.63	
MAC 781 nm	m^2 g^{-1}	5.78		8.02±1.56	

[a] Not simultaneously sampled with batch filter. [b]Batch filter and BC simultaneously sampled. [c]One standard deviation

636 **Table 3. Aircraft based measurements of fire average MCE and EF (±1 standard deviation)**

	Number of samples	MCE	$EFCO_2$ ($g\ kg^{-1}$)	EFCO ($g\ kg^{-1}$)	$EFCH_4$ ($g\ kg^{-1}$)
L1G	30[a]	0.950±0.016	1738±29	58.4±18.9	1.75±0.96
L2G	10[b]	0.953±0.005	1743±8	55.0±5.4	1.57±0.48
L2F	30	0.906±0.019	1651±37	108.4±21.4	4.32±1.58

637

638

639 [a]$EFCH_4$ is based on 21 samples. [b]$EFCH_4$ is based on 7 samples

640

641

642 **Figure Captions**

643

644 **Fig. 1.** Position of ground-based instruments relative to (*a*) L1G, (*b*) L2G, and (*c*) L2F. Yellow
645 dots indicate smoke monitors (EBAMs and CO monitors). White triangles indicate SLR and
646 video cameras. The black and yellow bulls eye at the north of each image indicates the location
647 of the Mets Tower background reference EBAM.

648

649 **Fig. 2.** The helium-filled tethered aerostat (4.3 m in diameter) and the light-weight instrument
650 package termed the "Flyer". Flyer instruments included SUMMA canisters for CO and CO_2;
651 batch sampling of $PM_{2.5}$ onto a 47-mm diameter Teflon filter (2 µm pore size, constant 10 L min^{-1});
652 batch sampling onto quartz filters for elemental carbon and organic carbon (EC and OC)
653 analyses; and a global positioning system.

654

655 **Fig. 3.** Two photographs taken at the same time but from different cameras during burn L2F: *(a)*
656 was taken by camera CA3, (*b*) by CA5, at positions indicated in Fig. 1.

657

658 **Fig. 4.** Airplane horizontal flight profile for fire L2F. The thick colour lines denote the flight
659 path at different altitudes in metres above sea level (m a.s.l): aqua (300 m a.s.l), blue (450 m
660 a.s.l.), purple (620 m a.s.l.), olive (910 m a.s.l.). The L2F burn unit is shown as a red polygon
661 and a 2 km x 2 km background grid is provided for reference.

662

663 **Fig. 5.** Airplane vertical flight profile for the L2F fire. The dashed black line is the airplane
664 altitude (in meters above mean sea level) and the red line is the CO mixing ratio (in parts per

million by volume) measured with the CRDS trace-gas analyser. The x-axis is time in 1000 seconds since midnight (ssm) (e.g. 44640 ssm is 12:24:00 CST).

Fig. 6. Ground-based 5-min and hourly $PM_{2.5}$ concentration averages as measured by the three of the nine EBAM monitors deployed that were impacted by smoke during L1G (grass burn). Numbers in the legend match numbers in Fig.1*a*. Ignition of the burn started at 1230 (USA CST) and ended at 1346 (USA CST).

Fig. 7. Box plot of ground based hourly $PM_{2.5}$ concentration averages as measured by the EBAM monitors deployed during the L2F (forest understory) burn. The prescribed burn ignition started at 1202 (USA CST) and ended at 1500 (USA CST). Median values are shown as the centre line across the box with the first and third quartile values as the lower and upper lines of the box, respectively. Whiskers extend to the minimum and maximum values.

Fig. 8. $PM_{2.5}$ emission factors for L2G (grass) and L2F (forest understory) burns derived from the mixing ratios measured with the ground and aloft batch filters (left). The error bar denotes a single standard deviation. Particle size distributions from continuous measurements during the L2G and L2F burns (right).

Fig. 9. Black carbon (BC), brown carbon (BrC) and elemental carbon (EC) emission factors derived from the L2G (grass) and L2F (forest understory) burns from mixing ratios sampled near the ground and aloft.

Fig. 10. Black carbon (BC) emission factors with respect to measured modified combustion

efficiency (MCE). Data from Aurell and Gullett (2013) also shown (red dots), these data were derived in an earlier study near the location of this study. The label 'Forest burn' in the figure indicates forest understory burn, similar to L2F of this study.

Fig. 11. Representative black carbon (BC) size distribution measured by the SP2 during the L2G (grass) and L2F (forest understory) fires. Data are fit with a lognormal distribution (solid lines) to determine the mass median diameter (MMD).

Fig. 12. One-minute averaged single scattering albedo (SSA) and BC/$PM_{2.5}$ ratio for the L2F (forest understory) fire.

Fig. 13. CRDS aircraft-based measurements of CO_2, CH_4, and CO mixing ratios for smoke sample run L2F03 of the L2F (forest understory) fire. The solid markers denote the data points used as the smoke sample. The horizontal dashed line in each panel shows the background mixing ratios measured in the smoke free air prior to plume penetration. The markers are two second data points plotted versus time given as 1000 seconds since midnight (ssm) CST, e.g. 44640 ssm is 12:24:00 CST.

Fig. 14. CRDS aircraft measured MCE (top) and $EFCH_4$ (bottom) plotted versus the estimated time of emission (ETE, see text) for the L2F (forest understory) fire. ETE is plotted in seconds since midnight (ssm) CST, e.g. 44640 ssm is 12:24:00 CST. Solid lines are linear least squares fits. The Spearman's rank correlation with ETE was $r = -0.48$ ($p < 0.01$) for MCE and $r = 0.80$ ($p < 0.0001$) for $EFCH_4$.

713 **Fig. 15**. Fire average MCE and $EFCH_4$ for the forest understory, L2F, fire (solid circle) and
714 previous study averages (solid squares) of MCE (left) and $EFCH_4$ (right). The previous studies
715 reported fire average EF for multiple fires and the whiskers denote the range of the fire average
716 EF from these studies. A13 = Akagi et al. 2013 with 7 fires; B11 = Burling et al. 2011 with 6
717 fires in North Carolina only; U09 = Urbanski et al. 2009 with 21 fires.
718
719

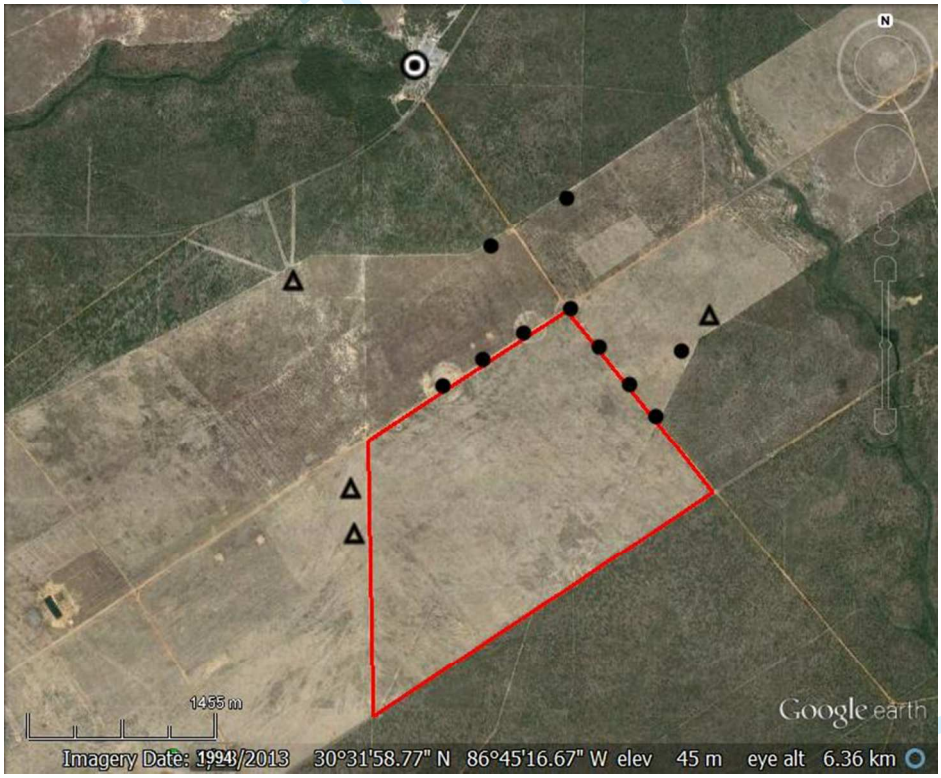

720
721

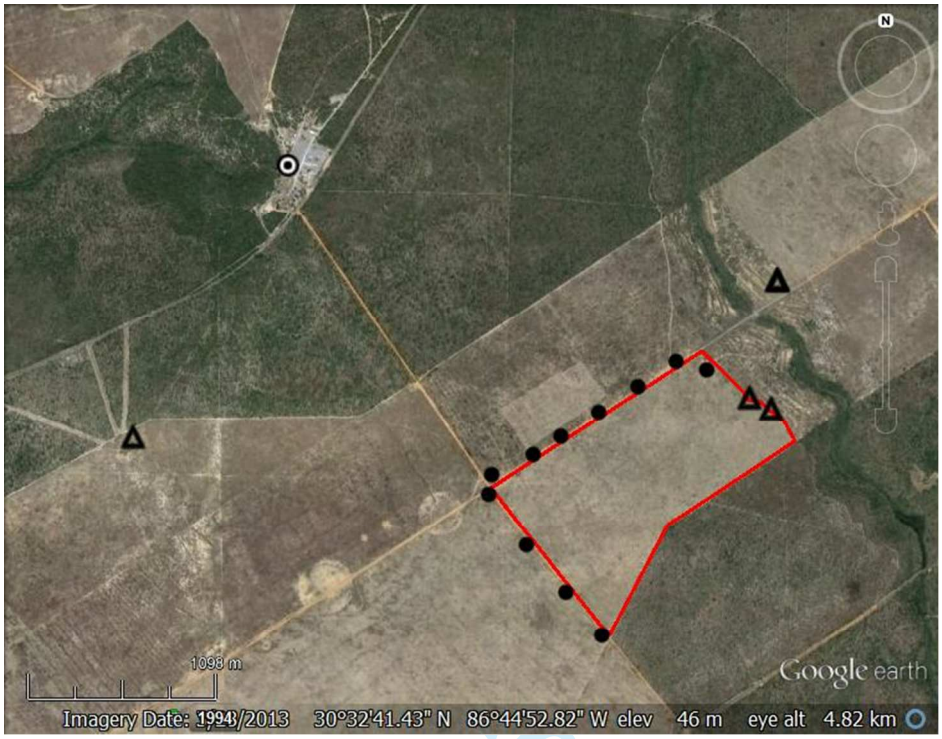

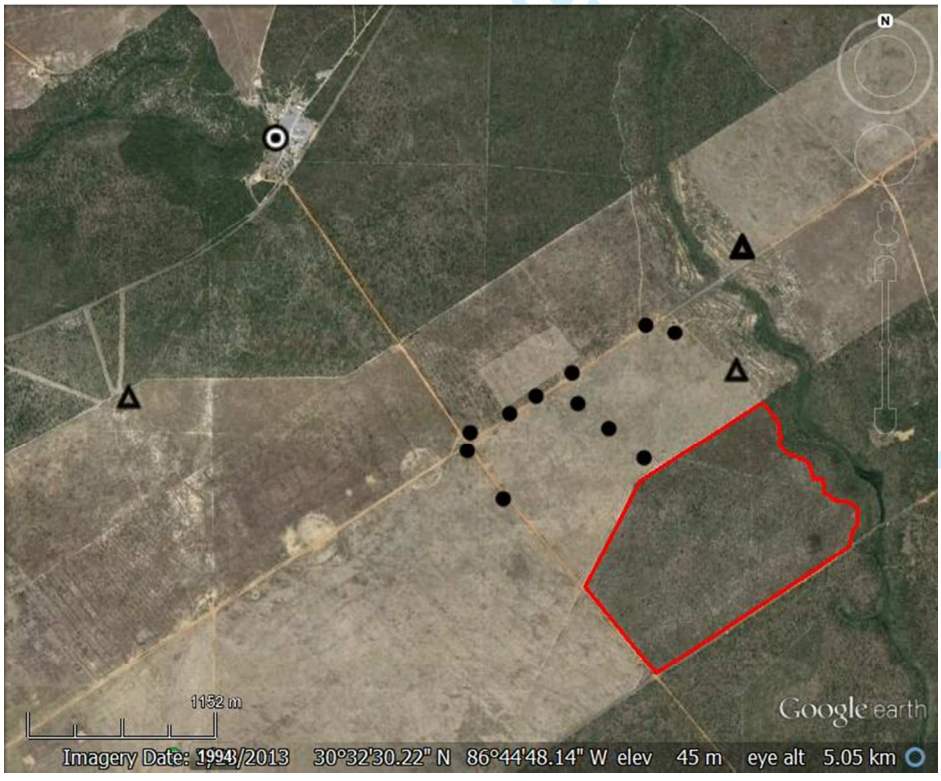

Figure 1a, b, and c.

726

727

728

729 Figure 2.

730

731

732 (a)

733

734 (b)

735 Figure 3.

736

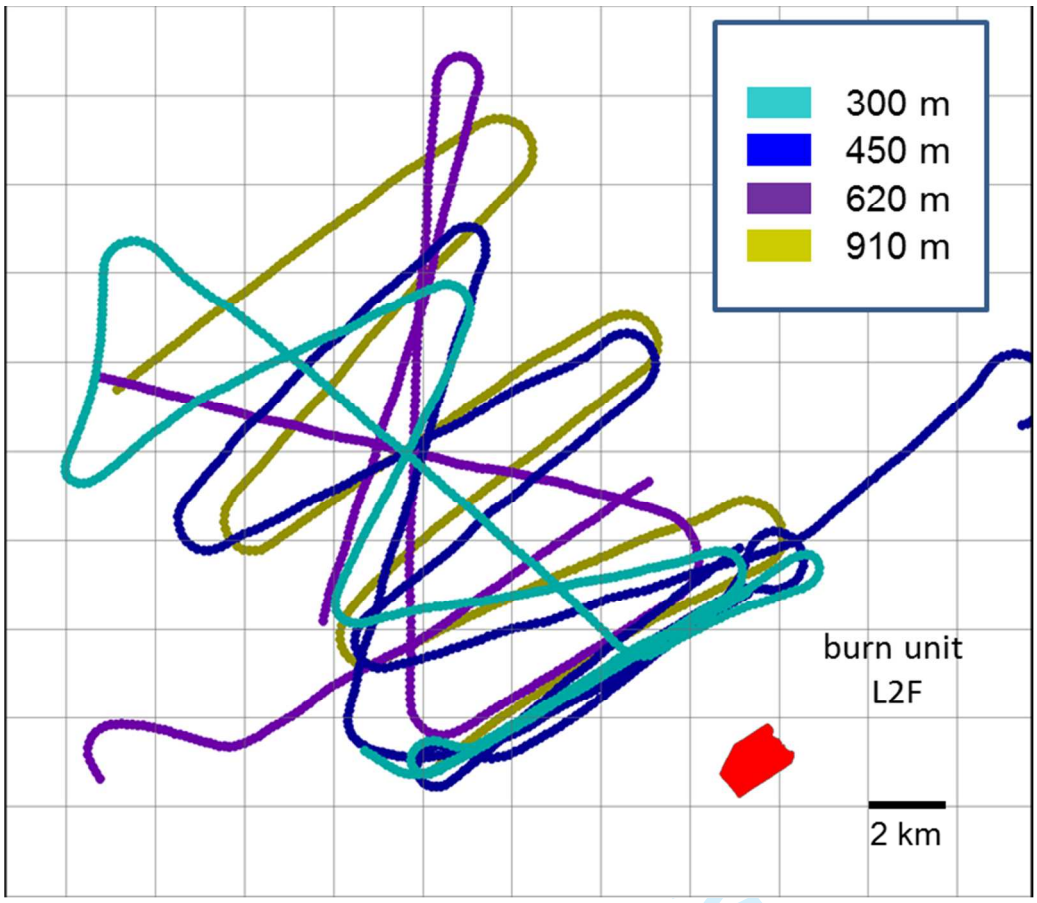

737

738

739 Figure 4.

740

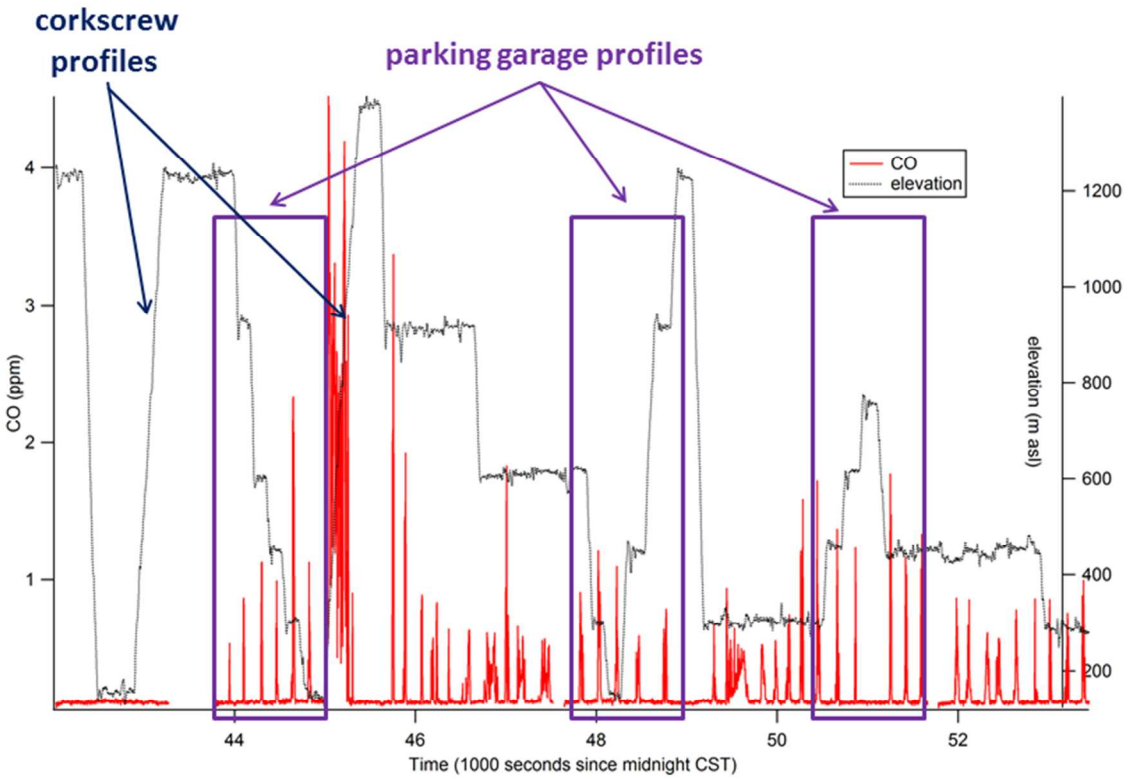
corkscrew profiles
parking garage profiles
CO
elevation
CO (ppm)
elevation (m asl)
Time (1000 seconds since midnight CST)
1
2
3
4
200
400
600
800
1000
1200
44
46
48
50
52

Figure 5.

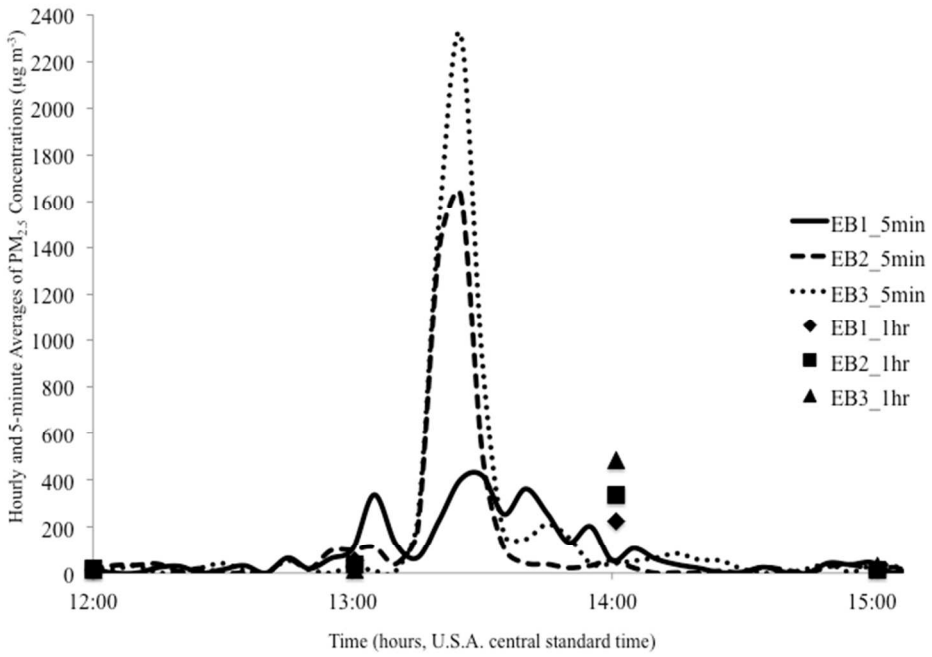

Figure 6.

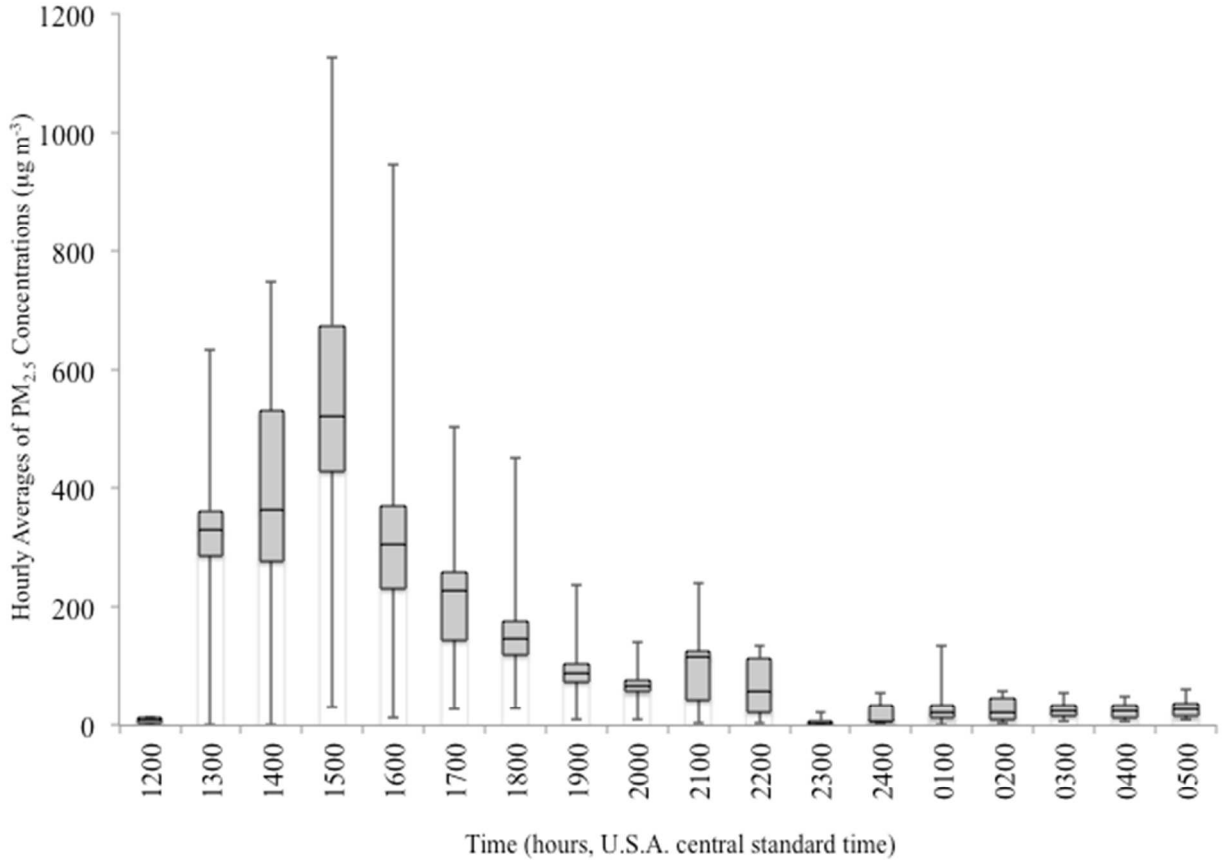
1200
1000
800
600
400
200
0
Hourly Averages of $PM_{2.5}$ Concentrations ($\mu g\ m^{-3}$)
1200
1300
1400
1500
1600
1700
1800
1900
2000
2100
2200
2300
2400
0100
0200
0300
0400
0500
Time (hours, U.S.A. central standard time)

Figure 7.

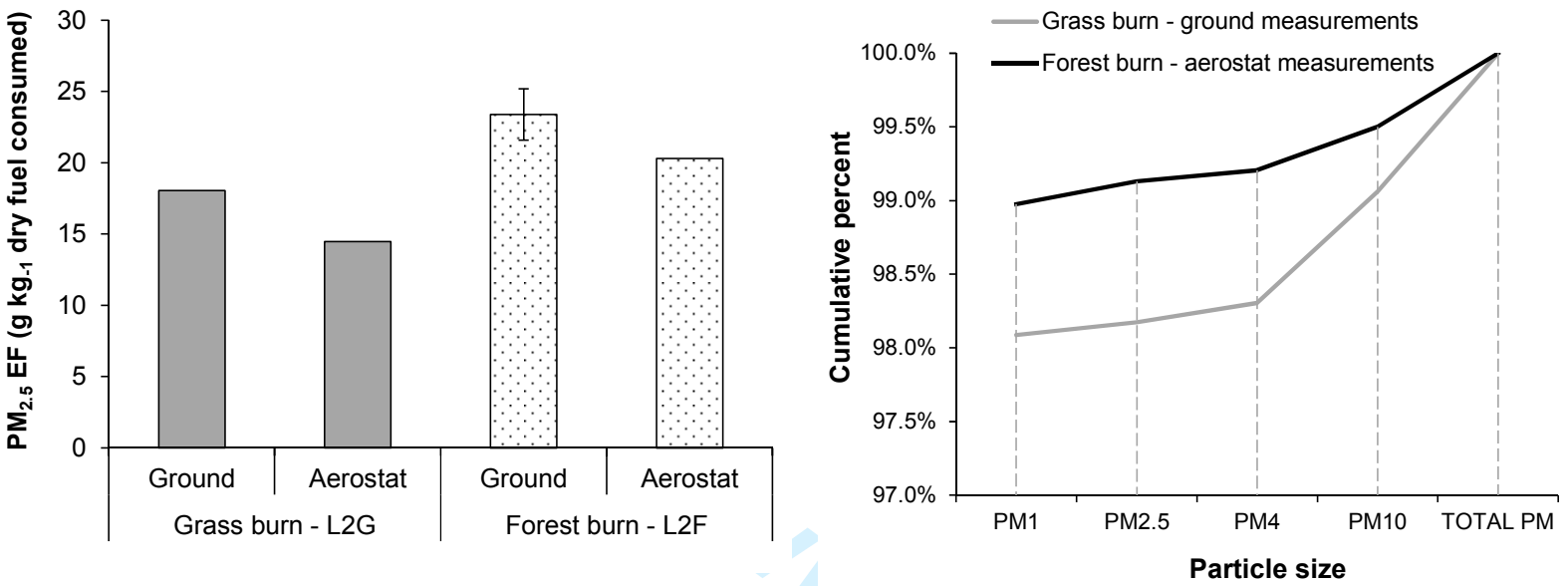

Figure 8.

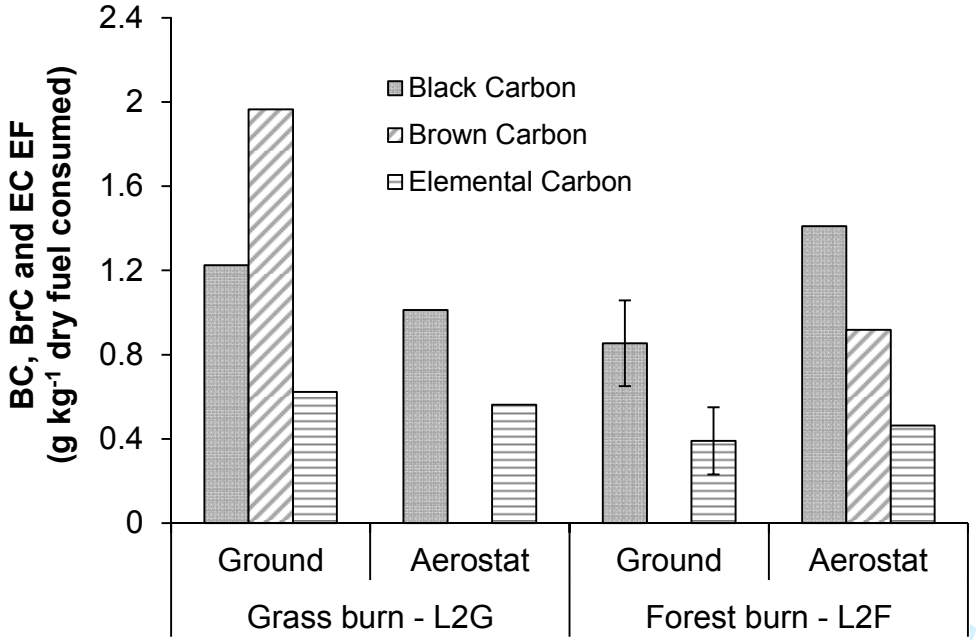

Figure 9.

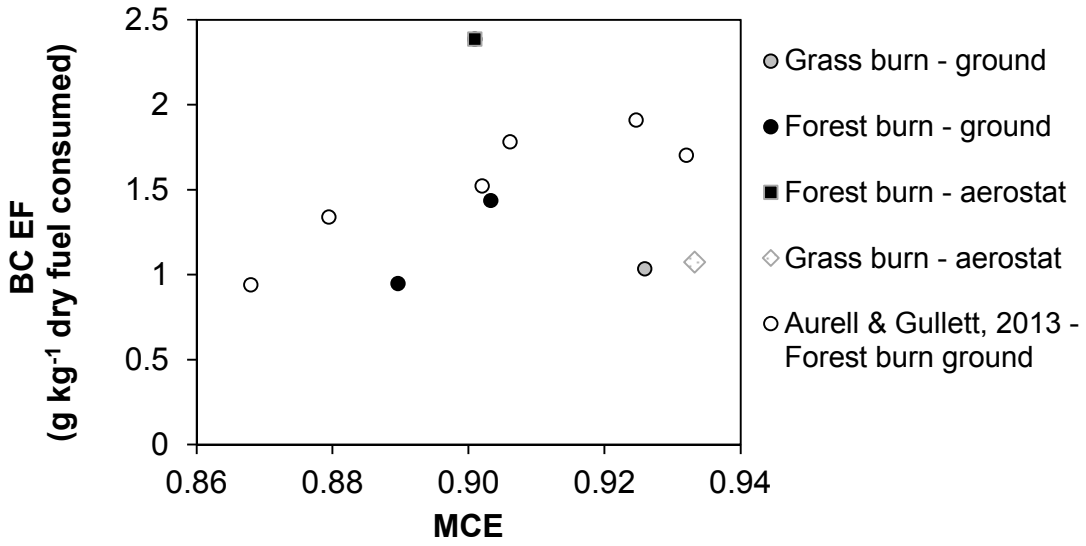

Figure 10.

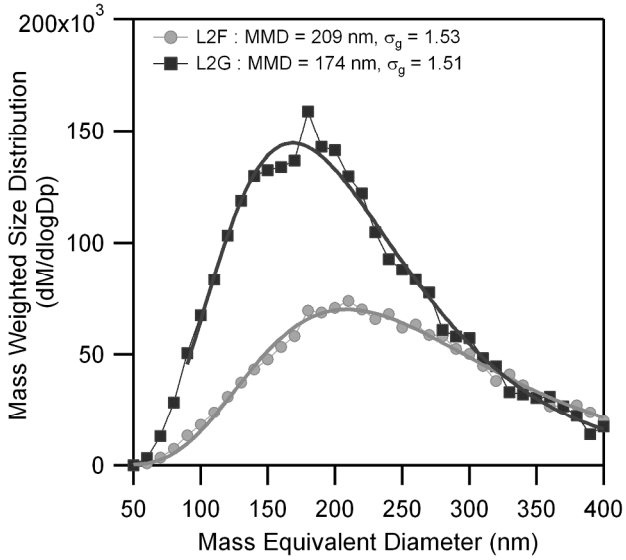

Figure 11.

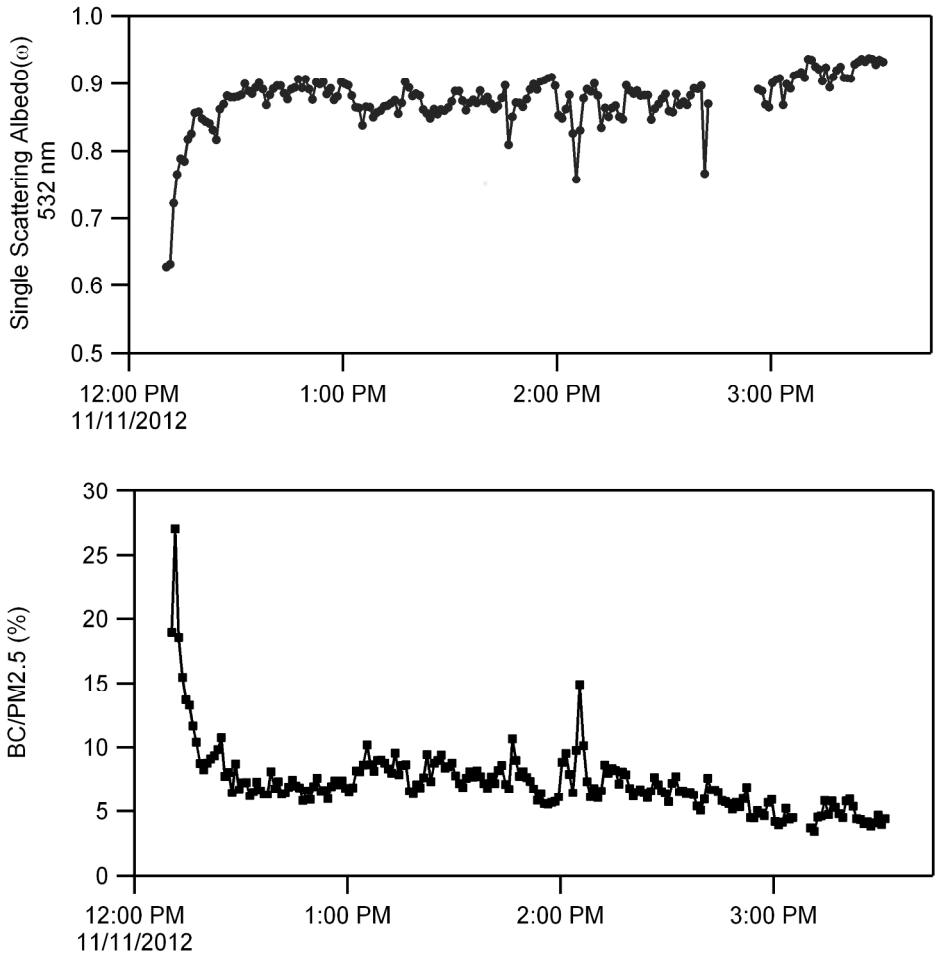

Figure 12.

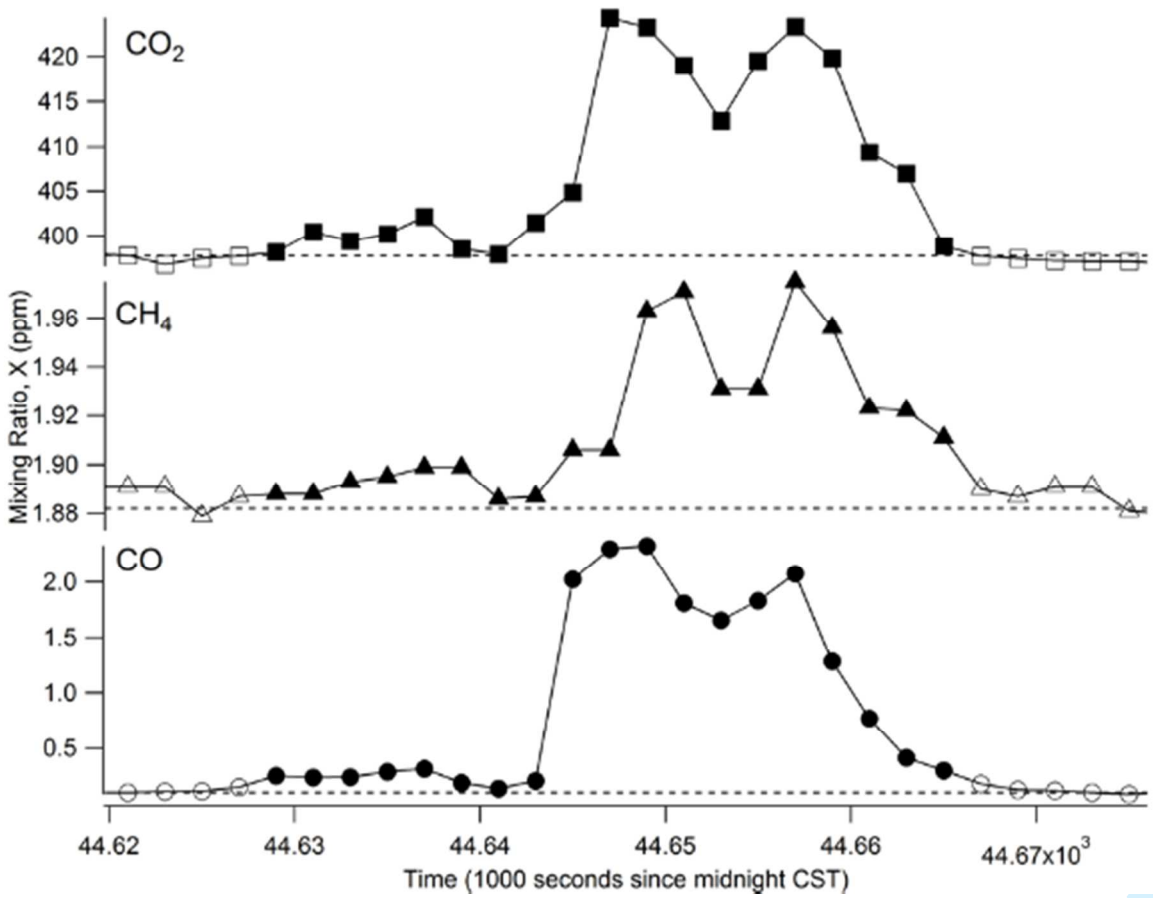
CO2
420
415
410
405
400
CH4
1.96
1.94
1.92
1.90
1.88
Mixing Ratio, X (ppm)
CO
2.0
1.5
1.0
0.5
44.62
44.63
44.64
44.65
44.66
44.67x10^3
Time (1000 seconds since midnight CST)

Figure 13.

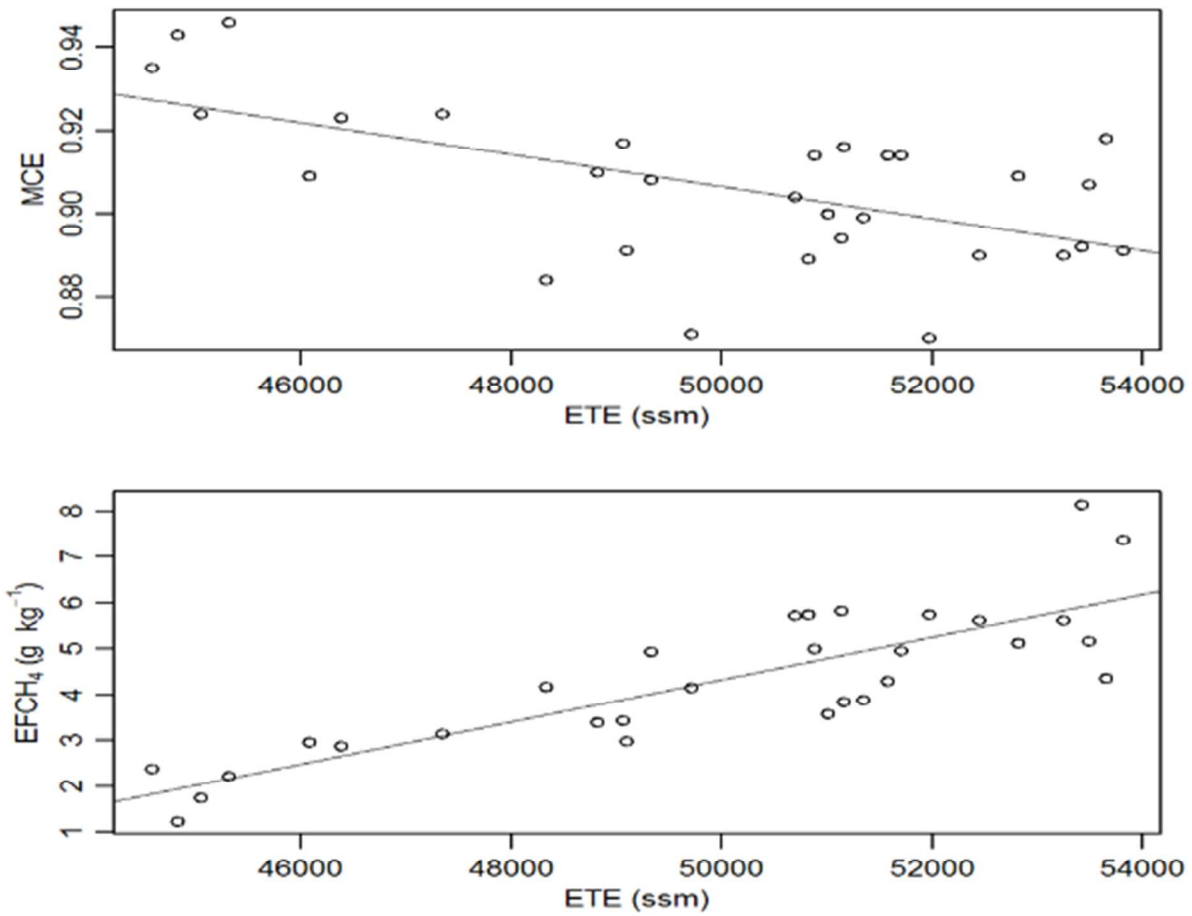
MCE
0.88
0.90
0.92
0.94
46000
48000
50000
52000
54000
ETE (ssm)
EFCH4 (g kg-1)
1
2
3
4
5
6
7
8
46000
48000
50000
52000
54000
ETE (ssm)

Figure 14.

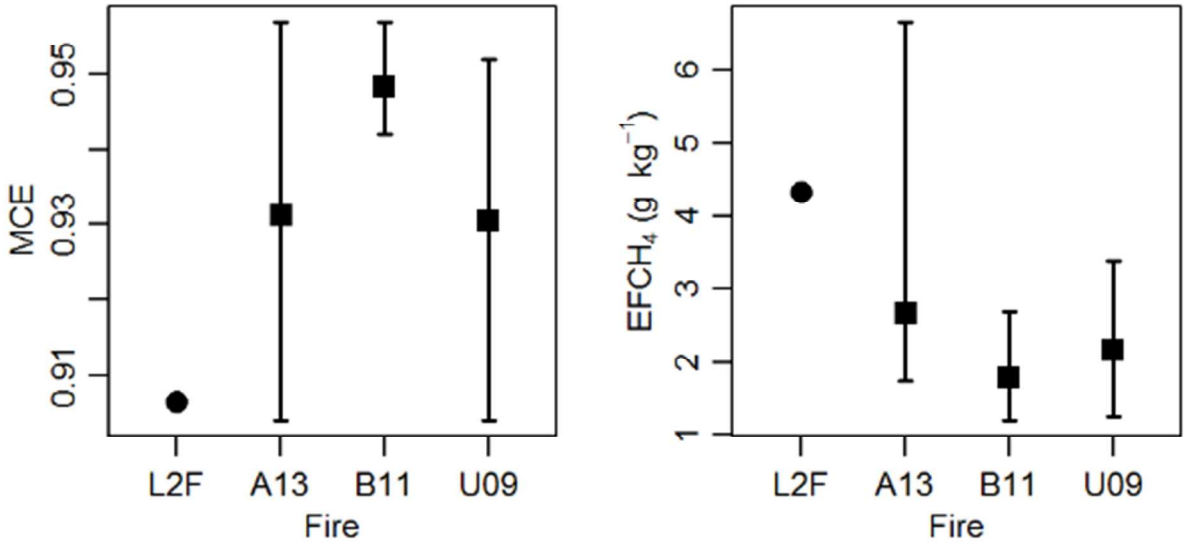

Figure 15.

Supplement

Table S1. Smoke sample ΔX, MCE, and EF and fire-average (± 1 standard deviation) MCE and EF

ΔX are average of the individual 2 s data points. An entry of "NA" indicates that the measured ΔX was not above the detection limit.

Sample	Altitude (m a.s.l.)	Est. emission time (ssm)	n	ΔCO_2 (ppmv)	ΔCO (ppmv)	ΔCH_4 (ppmv)	MCE	$EFCO_2$ (g kg^{-1})	EFCO (g kg^{-1})	$EFCH_4$ (g kg^{-1})
Fire L1G November 4, 2012										
LG101	353	46519	14	7.281	0.442	NA	0.943	1727	66.7	NA
LG102	337	46809	14	0.525	0.071	NA	0.881	1614	138.3	NA
LG103	615	46865	10	2.112	0.154	NA	0.932	1707	79.4	NA
LG104	616	47678	11	2.519	0.085	NA	0.967	1773	38.2	NA
LG105	629	47820	26	1.878	0.051	NA	0.974	1783	30.6	NA
LG106	647	47424	29	8.312	0.426	0.013	0.951	1741	56.8	1.01
LG107	646	47420	29	9.009	0.424	0.013	0.955	1748	52.4	0.95
LG108	1333	48228	24	10.530	0.531	0.026	0.952	1741	55.9	1.56
LG109	1391	48372	16	3.118	0.116	0.011	0.964	1762	41.7	2.27
L1G10	1271	48563	24	6.338	0.286	0.023	0.957	1748	50.2	2.27
L1G11	1102	48773	22	7.076	0.364	0.015	0.951	1740	57.0	1.35
L1G12	947	48973	25	4.704	0.237	0.008	0.952	1743	55.9	1.02

L1G13	622	49337	22	1.261	0.056	NA	0.957	1753	49.7	NA
L1G14	622	49337	22	1.297	0.061	0.004	0.955	1746	52.0	2.04
L1G15	330	49478	22	1.643	0.081	0.014	0.953	1733	54.6	5.25
L1G16	941	49635	30	4.036	0.203	0.007	0.952	1743	55.7	1.14
L1G17	941	49636	20	5.875	0.300	0.010	0.951	1741	56.6	1.07
L1G18	955	50032	28	2.211	0.113	0.007	0.951	1739	56.8	1.92
L1G19	943	50227	49	1.375	0.065	0.003	0.955	1747	52.3	1.48
L1G20	943	50135	37	1.647	0.081	0.005	0.953	1742	54.7	1.78
L1G21	945	50673	42	2.756	0.126	0.011	0.956	1746	50.9	2.50
L1G22	930	50673	13	2.887	0.135	0.008	0.955	1747	52.0	1.75
L1G23	950	50690	25	2.977	0.140	0.008	0.955	1747	52.3	1.68
L1G24	951	50846	49	1.908	0.086	0.007	0.957	1748	50.0	2.44
L1G25	936	51401	54	2.151	0.099	0.006	0.956	1748	51.0	1.76
L1G26	294	51160	8	8.179	0.365	0.011	0.957	1753	49.7	0.83
L1G27	277	50933	7	1.978	0.166	NA	0.923	1694	90.4	NA
L1G28	150	51321	10	9.435	0.613	0.011	0.939	1719	71.1	0.76
L1G29	151	51238	21	5.180	0.335	NA	0.939	1722	70.8	NA
L1G30	149	51433	9	4.550	0.234	NA	0.951	1746	57.1	NA
	Average						0.950±0.016	1738±29	58.4±18.9	1.75±0.96

Fire L2G November 10, 2012

L2G01	605	46354	26	7.030	0.325	0.011	0.956	1750	51.5	0.99
L2G02	757	46525	26	9.151	0.467	0.016	0.951	1738	58.7	1.13
L2G03	925	46882	24	11.220	0.642	0.027	0.946	1726	65.5	1.49
L2G04	1067	46991	32	12.254	0.650	0.032	0.950	1732	61.5	1.66
L2G05	1232	47113	23	6.980	0.346	0.019	0.953	1738	57.6	1.73
L2G06	1390	47494	27	12.079	0.595	0.029	0.953	1741	55.7	1.53
L2G07	1531	47838	20	1.635	0.062	0.006	0.963	1757	44.7	2.47
L2G08	915	49301	27	4.077	0.218	NA	0.949	1736	60.9	NA
L2G09	915	51225	52	2.666	0.129	NA	0.954	1746	53.9	NA
L2G10	917	51890	49	3.215	0.160	NA	0.953	1742	56.9	NA
	Average						0.953±0.005	1740±9	56.7±5.8	1.57±0.48
Fire L2F November 11, 2012										
L2F01	598	44586	11	7.461	0.518	0.029	0.935	1708	75.5	2.39
L2F02	450	44833	13	4.591	0.275	0.009	0.943	1726	65.9	1.23
L2F03	305	45039	24	8.373	0.693	0.024	0.924	1689	89.0	1.74
L2F04	151	45309	21	4.477	0.258	0.016	0.946	1728	63.3	2.22
L2F05	918	46082	13	13.418	1.338	0.066	0.909	1660	105.3	2.97
L2F06	916	46373	15	8.516	0.714	0.040	0.923	1684	89.9	2.89
L2F07	606	47340	26	5.243	0.429	0.027	0.924	1687	87.9	3.15
L2F08	621	48334	28	2.116	0.278	0.015	0.884	1610	134.7	4.17

L2F09	299	48815	25	3.781	0.374	0.021	0.910	1660	104.6	3.40
L2F10	145	49090	22	2.382	0.292	0.012	0.891	1626	127.0	2.98
L2F11	449	49060	22	2.264	0.206	0.013	0.917	1672	96.7	3.43
L2F12	915	49323	24	2.711	0.275	0.022	0.908	1652	106.8	4.95
L2F13	300	49715	22	0.689	0.102	0.005	0.871	1587	149.7	4.15
L2F14	307	51348	28	1.897	0.214	0.012	0.899	1638	117.6	3.89
L2F15	302	51131	26	1.317	0.156	0.013	0.894	1625	122.7	5.82
L2F16	306	50831	31	1.738	0.217	0.017	0.889	1616	128.5	5.74
L2F17	303	50700	20	4.854	0.518	0.047	0.904	1642	111.5	5.73
L2F18	458	51002	17	3.217	0.356	0.019	0.900	1642	115.6	3.59
L2F19	616	51158	10	3.715	0.339	0.023	0.916	1671	96.9	3.84
L2F20	298	50870	24	4.115	0.388	0.034	0.914	1663	99.8	5.00
L2F21	439	51573	13	6.165	0.580	0.044	0.914	1665	99.7	4.30
L2F22	441	51708	19	4.041	0.380	0.033	0.914	1663	99.4	4.97
L2F23	451	51962	23	3.028	0.452	0.030	0.870	1581	150.2	5.74
L2F24	431	52455	24	2.470	0.306	0.024	0.890	1618	127.4	5.63
L2F25	450	52815	29	1.908	0.192	0.016	0.909	1653	105.9	5.13
L2F26	436	53252	28	1.931	0.239	0.018	0.890	1617	127.6	5.62
L2F27	453	53481	27	2.243	0.229	0.019	0.907	1650	107.4	5.16
L2F28	289	53426	16	1.772	0.214	0.025	0.892	1616	124.1	8.14

L2F29	290	53643	26	2.078	0.186	0.015	0.918	1672	95.2	4.36
L2F30	283	53823	21	2.403	0.295	0.030	0.891	1615	126.2	7.38
	Average						0.906±0.019	1651±36.6	108.4±21.4	4.32±1.58